Two distinct ship emission profiles for organic-sulfate source apportionment of PM in sulfur emission control areas

Kirsten N. Fossum[1], Chunshui Lin[1,2,3], Niall O'Sullivan[4], Lu Lei[1], Stig Hellebust[4], Darius Ceburnis[1], Aqeel Afzal[1,5], Anja Tremper[6], David Green[6,7], Srishti Jain[4], Steigvilė Byčenkienė[8], Colin O'Dowd[1], John Wenger[4], and Jurgita Ovadnevaite[1]

[1]School of Natural Sciences, Ryan Institute's Centre for Climate & Air Pollution Studies, University of Galway, Galway, H91 CF50, Ireland
[2]State Key Laboratory of Loess and Quaternary Geology and Key Laboratory of Aerosol Chemistry and Physics, Chinese Academy of Sciences, 710061, Xi'an, China
[3]Department of Civil and Environmental Engineering, the Hong Kong Polytechnic University, Hong Kong, China
[4]School of Chemistry and Environmental Research Institute, University College Cork, Cork, Ireland
[5]Institute of Energy and Environmental Engineering, University of the Punjab, Lahore, Pakistan
[6]MRC Centre for Environment and Health, Environmental Research Group, Imperial College London, UK
[7]NIHR HPRU in Environmental Exposures and Health, Imperial College London, UK
[8]SRI Center for Physical Sciences and Technology, Lithuania

Correspondence to: Jurgita Ovadneviate (jurgita.ovadnevaite@universityofgalway.ie)

Abstract. Source apportionment quantitatively links pollution to its source, but can be difficult to perform in areas like ports where emissions from ship and other port-related activities are intrinsically linked. Here we present the analysis of aerosol chemical speciation monitor (ACSM) data and combined organic and sulfate ion positive matrix factorization (PMF) during an intensive measurement campaign in Dublin Port. Two main types of ship emissions were identified by this technique: sulfate-rich (S-Ship) and organic-rich (O-Ship). The S-Ship emissions were attributed to heavy fuel oil use and are characterised by particles with standard V/Ni ratios from 2.7-3.9 and a large fraction of acidic sulfate aerosol. The O-Ship emissions were attributed to low-sulfur fuel types and were comprised mostly of organic aerosol (OA) with the V/Ni ratios ranging only from 0-2.3. O-Ship plumes occurred over three-times more frequently than S-Ship plumes during the measurement period. Ship plumes had PM_1 concentrations in the range 4 - 252 µg m^{-3}, with extreme concentrations usually lasting for 5-35 minutes. A third minor ship emission factor (X-Ship) was resolved by PMF, but not clearly attributable to any specific fuel type. Despite their short duration, shipping emission plumes were frequent and contributed to at least 28% of PM_1 (i.e. 14% O-Ship, 12% S-Ship, and 2% X-Ship). Moreover, hydrocarbon-like organic aerosol (HOA) and black carbon could also originate, at least in part, from ship emissions and shipping related activities, suggesting that the shipping contribution to ambient PM is likely higher, with a maximum of 47%.

1 Introduction

Shipping traffic is set to expand worldwide increasing pollution in port areas and potentially leading to poorer air quality for 40% (2.4 billion people) of the world's population living within 100 km of the coast. A range of emission sources influence the air quality in port areas, including combustion sources such as ocean-going vessels, heavy goods vehicles and land-based industry. These emissions have many similar chemical components, and it can be difficult to separate individual sources, especially when they may be intrinsically related e.g., primary ship emissions and secondary formation of aerosol from ship related precursor gases. However, a combination of chemical analysis methods and source apportionment modelling can be used to successfully determine the contribution of specific sources to the ambient particulate matter measured in port areas. For example: 3.7–6.1% of organic aerosol was related to shipping and industrial plumes in Marseille, France (Chazeau et al., 2022), 1.5% of $PM_{2.5}$ and 18% of particle number concentration was related to shipping traffic in Cork Harbor, Ireland (O'connor et al., 2013; Healy et al., 2010), shipping emissions were 5–14% of $PM_{2.5}$ in Spanish coasts (Pandolfi et al., 2011; Viana et al., 2009) and were 4–13% of primary $PM_{2.5}$ in Shanghai Port and Hong Kong Ports (Yau et al., 2013; Zhao et al., 2013) and 25% overall in Hong Kong Port (Yau et al., 2013). In Ningbo-Zhoushan Port, China, 18% of polycyclic aromatic hydrocarbons (PAHs) in $PM_{2.5}$ were found to come from heavy fuel oil combustion (Hong et al., 2023), and shipping emissions contributed 6–22% of volatile organic compounds in the Pearl River Delta region (Tong et al., 2024).

High time resolution measurements of aerosol chemical composition can be used to identify different emission sources in port areas as they are capable of reflecting the transient emission sources and changing meteorology. For example, Vanadium (V) and Nickel (Ni) have been used as chemical tracers to identify primary emissions from combustion of Heavy

Fuel Oil (HFO) (Healy et al., 2009; Mueller et al., 2011; Agrawal et al., 2009; Zhao et al., 2013) and concentration ratios of

60   V/Ni ranging from 2.5–4 are associated with typical ship emissions (Mazzei et al., 2008; Pandolfi et al., 2011; Viana et al., 2009). Different analysis techniques can be used to perform source apportionment; one leading type of multivariate analysis for high-resolution aerosol composition is positive matrix factorisation (PMF). PMF is capable of resolving distinct primary as well as secondary aerosol sources (*e.g.* Chazeau et al., 2022; Yau et al., 2013).

There are many regulations and guidelines related to the control of emissions and air quality in port areas. Among these are

65   sulfur emission control areas (SECA), which aim to reduce emissions of sulfur oxides from marine sources by limiting the sulfur-content in marine fuel. These regulations are enforced in Europe through the EU Sulfur Directive and at the international level by the International Maritime Organisation (IMO). On January 1st, 2015, the IMO reduced the limit on sulfur fuel content in SECA from 1.0% m/m (mass by mass) to 0.1% m/m. Additionally, the maximum sulfur content outside of SECA was reduced from 3.5% m/m to 0.5% m/m on January 1st, 2020 (IMO 2020). Due to the higher cost of low-sulfur

70   (low-S) fuels, many ship operators have instead installed exhaust scrubber systems, which reduce the gaseous sulfur emissions. A common wet scrubber design uses alkaline solution, often seawater pumped from below the ship, to spray through the ship exhaust, scavenge, and reduce gaseous SO_2 emissions. Vessels with exhaust scrubber systems, in accordance with an amendment to the original regulations, are still allowed to use fuels exceeding 0.50% sulfur after March 1st 2020. These systems can be open or closed, with the open system cycling in seawater to use for scrubbing and cycling out

75   the sulfur enriched scrubbing water back into the sea. This has many implications for both the composition of the aerosol emissions and for seawater acidification and pollution. The transition from HFO (S<3.5%) to low-S fuel (0.1% m/m) has been shown to reduce the mass concentration of particulate matter (PM) by 67%, reduce SO_2 emissions by 80% and lead to an overall decrease in volatile organic compounds, including the heavier and carcinogenic PAHs, but an increase in the production of monoaromatic and lighter polyaromatic hydrocarbon compounds (Zetterdahl et al., 2016). However, it is

80   reported that the reduction in sulfur fuel content is unlikely to lead to significant changes in either the total particle number concentration or the black carbon mass concentration (Zetterdahl et al., 2016). Studies have pointed out that low-S fuels contain much lower amounts of metals from the refinery process and therefore will not have the typical chemical markers of HFO traditionally used for tracing ship emissions (Anders et al., 2023; Czech et al., 2017). While it has been proposed that lubricant oil from marine engines could provide a fuel-independent pool of possible marker substances (Eichler et al., 2017),

85   new studies are urgently needed in port areas to derive alternative markers or chemical profiles for ship emissions, as well as diagnostic ratios for both particle-bound and volatile organics (Czech et al., 2017).

Dublin Port is the largest port in Ireland, classified as a Tier 1 medium port. In 2019, it handled 49.5% (~26.3 million tonnes) of Irish Freight (Transport Omnibus (2019). For context, the largest port in the EU, Rotterdam Port, has 18-times this capacity. Dublin Port expects to double its capacity by 2040, at a 3.3% expansion rate per annum (Dublin Port Masterplan

90   2040 (Dpc, 2018)). Dublin Port is adjacent to the urban centre of Dublin city (< 5 km), where the air quality has been studied at both background and roadside monitoring locations (Lin et al. 2018, Lin et al. 2019, Ovadnevaite et al. 2021). Dublin is known to be diurnally affected by poor air quality arising from the burning of domestic solid fuels for home heating during

the colder (mainly winter) months, often with night-time peaks exceeding 100 µg m^{-3} (sometimes > 300 µg m^{-3}) for several hours (Lin et al. 2018, Ovadnevaite et al. 2021). Dublin Port is directly downwind of the prevailing Westerlies (South-Westerlies) and as such is impacted by both the air pollution from the Port and the City Centre of Dublin. As Dublin Port is a SECA, ships either switch to ultra-low-S content (0.1% m/m) fuels while at dock or else implement the use of scrubbers aboard the ship to reduce SO$_2$ emissions from burning fuels with higher S content. The resultant particulate emissions from the use of scrubbers would have the same V/Ni signatures of HFO, while supporting the rapid aqueous phase formation of acidic sulfate (SO$_4^{2-}$) within the plume stacks. In fact, studies of before and after scrubber system installation confirm the presence of SO$_4^{2-}$ in the aerosol particle phase from ship stacks with scrubbers (Yang et al., 2021). Conversely, ultra-low-S fuels as well as Very Low Sulfur Fuel Oil (VLSFO < 0.5% m/m) lack the processing that yield metal tracers (V/Ni) from the combustion of the fuel. The most common fuel use behaviours at Dublin Port were (i) using ultra-low-S fuels only (mainly Marine Gas Oil (MGO)), (ii) using VLSFO to power the engines and MGO for electricity generators when in port, (iii) using HFO for engines (with scrubber) and MGO for generators when in port, and (iv) using HFO with a wet scrubber operated using a closed loop system all the time.

A research project, *Source Apportionment of Air Pollution in the Dublin Port Area* (PortAIR), was initiated to measure the aerosol physical and chemical properties in the port area and assess the impact of Dublin Port activities on air quality before it doubles capacity by 2040. The PortAIR project comprises a 14-month long air quality field campaign (December 2021 – February 2023) and an 8-week long intensive measurement campaign (December 2022 – February 2023) at a monitoring site in Dublin Port, situated ~5km from the city centre. Here we present results from a 1-month period of the intensive campaign conducted in winter, when air quality was affected both by burning of domestic solid fuels in the city and by peak port activity from goods importation. The comprehensive range of instruments deployed at the monitoring site allowed characterisation of individual ship plumes and classification according to type of fuel used.

2 Methods

2.1 Measurement campaign

This study focuses on an intensive field measurement campaign in Dublin Port where aerosol physico-chemical properties and gaseous pollutants were measured using a suite of instrumentation housed in two containers. The intensive campaign ran from 16 December 2022 through to 7 February 2023. The monitoring site (latitude of 53.348439 and longitude of -6.194657) was selected to be downwind of most port activity and close to the ferries, which are a major daily source of shipping emissions. The location of the monitoring site in relation to the ferry terminals and other areas of the port is shown in Supplementary Fig. S1, along with a photograph of the two containers *in situ*.

High time resolution chemical composition data from a monitoring site around 5 km from Dublin Port is also used in this study. The site is at University College Dublin (UCD) (53.3089, -6.2242), an urban background location just South of Dublin city centre, close to main roads and residential areas.

2.2 Instrumentation

2.2.1 Meteorology

Wind direction, wind speed, air temperature, air pressure, relative humidity, rainfall and solar radiation measurements were made using a *Casella* weather station (model Nomad, UK) mounted to the top of the main container. The measured wind speed and direction compared well with the data available from the nearest Met Éireann meteorological station located at Dublin Airport, less than 10 km North of Dublin Port.

2.2.2 Q-ACSM

A PM_1 quadrupole aerosol chemical speciation monitor (Q-ACSM) from *Aerodyne Inc.* (Billerica, MA, USA) measured the mass concentrations of non-refractory species including organic aerosol (OA), sulfate (SO_4^{2-}), nitrate (NO_3^-), ammonium (NH_4^+) and chloride (Cl^-) (Ng et al., 2011). While the intensive campaign ran from 16 December 2022 to 7 February 2023, Q-ACSM data is only available through to January 27, 2023. The Q-ACSM used in the study had a standard vaporiser and was calibrated and maintained following the standard protocol developed by the Cost Action CA16109, COLOSSAL. Details of the Q-ACSM instrument can be found in previous studies (e.g. Ng et al. (2011) and Pieber et al. (2016)). In this study, the Q-ACSM was installed with a $PM_{2.5}$ URG-2000-30ED cyclone connected to 3/8 inch stainless steel tubing and operated using a carrier flow rate of 2.5 (±0.2) LPM with a distance from inlet to Q-ACSM of approximately 2 meters, to keep particle losses to a minimum. A monotube Nafion® membrane dryer was installed to maintain relative humidity (RH) of the sample air in the range 20–40%. The instrument was operated at a time resolution of just over five minutes (five sets of one sample and one filter measurement scans). The response factor (RF) of NO_3^- and relative ionization efficiencies (RIE) of NH_4^+, and SO_4^{2-} were determined following standard operating procedures (COLOSSAL) for ammonium nitrate and ammonium sulfate calibration. OA RIE was experimentally determined through comparison with another PM_1 Q-ACSM combined with use of a state-of-the-art organic RIE calibration with organic alcohols recommended by the Q-ACSM manufacturer. An RF of 2.81×10^{-11}, NH_4^+ RIE of 4.15, SO_4^{2-} RIE of 0.61, and organic RIE of 1.9 (standard is 1.4) was applied after validation during data ratification in the standard Q-ACSM data analysis process. Composition dependent collection efficiency (CDCE) was applied following the (Q-ACSM modified) methods of Middlebrook et al. (2012). The uncertainty in the mass concentration of the non-refractory species is considered ±30%. The 30-min average limits of detection for the Q-ACSM were calculated to be 0.110 µg m^{-3} for NO_3^-, 0.175 µg m^{-3} for SO_4^{2-}, 0.662 µg m^{-3} for NH_4^+, 0.561 µg m^{-3} for OA, and 0.105 µg m^{-3} for Cl^-, following the methods of Ng et al. (2011).

2.2.3 Aethalometer AE33

The dual-spot aethalometer (Model AE33, Magee Scientific) operates seven different wavelength channels (370, 470, 520, 590, 660, 880, and 950 nm) to provide optical absorption coefficients by measuring light attenuation every minute through a filter tape that has collected aerosol at a flow rate of 5 (±0.4) LPM. The AE33 Dual Spot^{TM} measurement technique allows for the correction of filter loading effects by aerosol in real-time (Drinovec et al., 2015). The 880 nm wavelength channel is classically used to measure light absorbing equivalent black carbon (eBC) (Petzold et al., 2013; Bond et al., 2013), using the standard mass-specific absorption cross section (MAC) of 7.77 m^2/g (Magee Scientific Inc. (2018); Drinovec et al., 2015). The rolling 15-min average was calculated from the 1-min data to reduce noise. This rolling average was used to interpolate eBC concentrations that matched Q-ACSM data points in time.

2.2.4 Xact 625

The Xact 625 (Xact, from this point onward) can measure up to 24 elements between silicon and uranium at hourly time resolution and has been evaluated and described in previous studies (Furger et al. (2017); Tremper et al. (2018)). The instrument has a flow rate of 1 m^3 h^{-1}; the inlet tube is heated to 45 °C when the ambient relative humidity (RH) exceeds 45%, which was usually the case. The samples are collected onto Teflon tape and subsequently analysed using energy dispersive X-ray fluorescence (EDXRF). The X-ray source used is a Rhodium anode (50 kV, 50 Watt) and the x-ray fluorescence is measured using a silicon drift detector. In this study, the instrument measured the elements As, Ba, Ca, Cd, Ce, Cl, Cr, Cu, Fe, K, Mn, Mo, Ni, Pb, Pt, S, Sb, Se, Si, Sr, Ti, V and Zn in PM$_{2.5}$. Daily automated quality assurance checks were performed at midnight. Further quality assurance checks, such as flow checks and external calibration checks were performed at the start and end of the campaign.

2.2.5 Gas analyzers

Nitrogen oxides (NO$_x$) and sulfur dioxide (SO$_2$) were measured throughout the campaign using automated gas analyzers. The NO$_x$ is measured by the *Teledyne Instruments* Chemiluminescent NO/ NO$_2$/ NO$_x$ Analyzer Model 200A which measured NO and NO$_x$ and by calculation NO$_2$ at 5-min time resolution. The total NO (NO$_x$) can be measured and are taken as parts per billion (ppb), and NO$_x$ is converted to µg m^{-3} as NO$_2$ ppb*1.9125 = NO$_2$ µg m^{-3}, and NO ppb*1.28 = NO µg m^{-3} (20°C, 1 atm). The SO$_2$ was measured at 1-min time resolution by a *Teledyne API* Model T100 UV Fluorescence SO$_2$ Analyzer that was used throughout the PortAIR project. A small drift in the SO$_2$ baseline was observed over the yearlong campaign, so the measurements were subsequently corrected using a polynomial function for baseline drift derived from laboratory tests conducted at the end of the campaign.

2.2.6 SMPS

The scanning mobility particle sizer (SMPS) characterises the number-size distribution of the ambient aerosol particles. Particles passing through the system are charge neutralized (Fuchs, 1963) (electrical ionizer model 1090, *MSP*) and then sized by electrical mobility through a differential mobility analyser (DMA, *TSI Inc.* model 3080) and finally counted by a condensation particle counter (CPC, *TSI Inc.* model 3010). The SMPS was operated by passing sample air through a multi-tube Nafion® membrane and into the DMA at a sample flow of ~ 1 LPM with a sheath flow of 5 LPM (Collins et al., 2004). The SMPS was operated at 3-5 min scan duration with *TSI Inc.* AIM software (release version 9.0.0.0) with charge correction applied.

2.3 Source apportionment

Positive matrix factorization (PMF; (Paatero, 1997)) was used to apportion the organic aerosol (OA) measured by the Q-ACSM into different emission source categories. The PMF was conducted on the original 5-min time resolution data using the multilinear-engine (ME-2; (Paatero, 1999)) implemented in the software SoFi (version 9.4.10) (Canonaco et al., 2013). PMF can be expressed by the bilinear factor model (Paatero and Tapper, 1994):

$$X_{ij} = G_{ik}F_{kj} + E_{ij}$$

Where for Q-ACSM data, *X* is the measured mass spectrum over time (including negative and zero values) with dimensions $i \times j$, *G* is the time series of non-negative factors ($i \times k$; k is the number of factors), *F* is the non-negative factor profiles ($k \times j$), and *E* is the residuals of the model with the same dimensions as *X*. The least squared algorithm was employed to minimize the value of Q (sum of squared residuals weighted by respective uncertainties), ensuring a good fit between the model and observed data (Canonaco et al., 2013; Crippa et al., 2014).

In this study, unconstrained PMF solutions were first considered (see Supplementary Fig. S2), but did not yield any physically meaningful separation of factors. Reference mass spectral profiles were used to constrain the ME-2 algorithm (Canonaco et al., 2013) and these reference profiles were left to vary within specified limits using the limits approach (Lin et al., 2021). Different from the a-value approach where all *m/z* in the mass spectrum vary uniformly, in the limits approach, each *m/z* in the input mass spectrum was individually varied. For example, one *m/z* may have a variation of 2% while another may vary by 40%. This approach is commonly used to capture variation in emission conditions, such as different stove type for burning solid fuels, and can be found when combining multiple profiles into a mean mass spectrum with standard deviations (σ_j) at each ion (m/z_j). The limits were then set for each *m/z*, with the lower limit ($\overline{m/z}_j - \sigma_j$) and upper limit ($\overline{m/z}_j + \sigma_j$). To assess the robustness of the PMF solution, a Bootstrap resampling strategy was employed (Paatero et al., 2014; Ulbrich et al., 2009; Davison and Hinkley, 1997; Efron, 1979). This method evaluated the statistical uncertainty of the solution, which could, e.g., arise from variations in emission sources.

For the PMF analysis, an inorganic and organic combined matrix was employed, which combined OA ions and directly measured fragment ions for SO_4^{2-} for an organic-sulfate input matrix. The OA mass spectrum was extended up to m/z 120 and additional columns were added for SO_4^{2-}. The error matrix for these ions was generated using the same initial error

215 calculation as for OA. The organic-sulfate input was down weighted cell-wise based on the signal to noise ratio (SNR), where bad or weak signals with SNR<0.2 (negative and zero included) or SNR<2, respectively, are down weighted by being given higher error values. in SoFi Pro. Overall, the calculated SNR for the sulfate ions shows that m/z 81 for HSO_3^+ and m/z 98 for $H_2SO_4^+$ are weak (Fig. S3). Additionally, the CO_2 related OA m/z 16, 17, and 18 were removed to run the PMF but were added back in later using known fragmentation patterns (Chen et al., 2022; Canonaco et al., 2021; Parworth et al.,

220 2015). The SO_4^{2-} fragment ions included were m/z 48 for SO^+, m/z 64 for SO_2^+, m/z 80 for SO_3^+, m/z 81 for HSO_3^+, and m/z 98 for $H_2SO_4^+$ (Sun et al., 2012). Since these ions only account for about 54% of the measured SO_4^{2-} (Fig. S4a), the remaining SO_4^{2-} was added back in later to the factors containing SO_4^{2-}. The remaining ion fragments for SO_4^{2-} were calculated based on the ion ratio to m/z 80. This ratio was chosen as this is the m/z value with non-weak SNR that shows the most variation between neutralised and acidic SO_4^{2-} (Chen et al., 2019) and that varied over the intensive campaign between

225 neutralised SO_4^{2-} regional episodes and the acidic SO_4^{2-} in plumes (discussed further in the supplementary material). The organic-sulfate input was well captured by the PMF solution, with a slope between factor mass concentration and input of 1.03 (Fig. S4b).

3 Results and discussion

An overview of the high time resolution data from the intensive campaign is shown in Fig. 1. Many high pollution events of

230 short duration were observed, with the peak PM_1 mass concentration reaching 252 µg m^{-3}. The pollution events typically lasted 5-35 minutes and were driven by OA, often in combination with SO_4^{2-} and other inorganic species. Elemental sulfur (S), vanadium (V), and nickel (Ni) were also present during pollution plumes that contained SO_4^{2-}. While the V/Ni ratio was often in the range 2.5-4.0 (Fig. 1), consistent with HFO emissions (Viana et al., 2009; Pandolfi et al., 2011), an appreciable number of pollution spikes had a V/Ni ratio less than 2.5, suggesting use of a different fuel type in the Port area. The spikes

235 in PM_1 occurred in conjunction with increased SO_2 and NO_x concentrations, and enhanced aerosol number concentration (d_p =10-500 nm). However, enhanced number concentration did not always result in very high mass concentrations of the aerosol as they were driven by smaller diameter aerosol particles (e.g. Fig. S5). The very local nature of these pollution spikes is verified by comparing the results with those obtained at the urban background site (UCD) where a PM_1 Q-ACSM and AE33 were deployed. The comparison (Fig. S6) shows that while some regional pollution events occur simultaneously

240 at both sites, the pollution spikes at Dublin Port are unique and localised. Source apportionment was, thus, used to identify the origins of these short-lived pollution episodes.
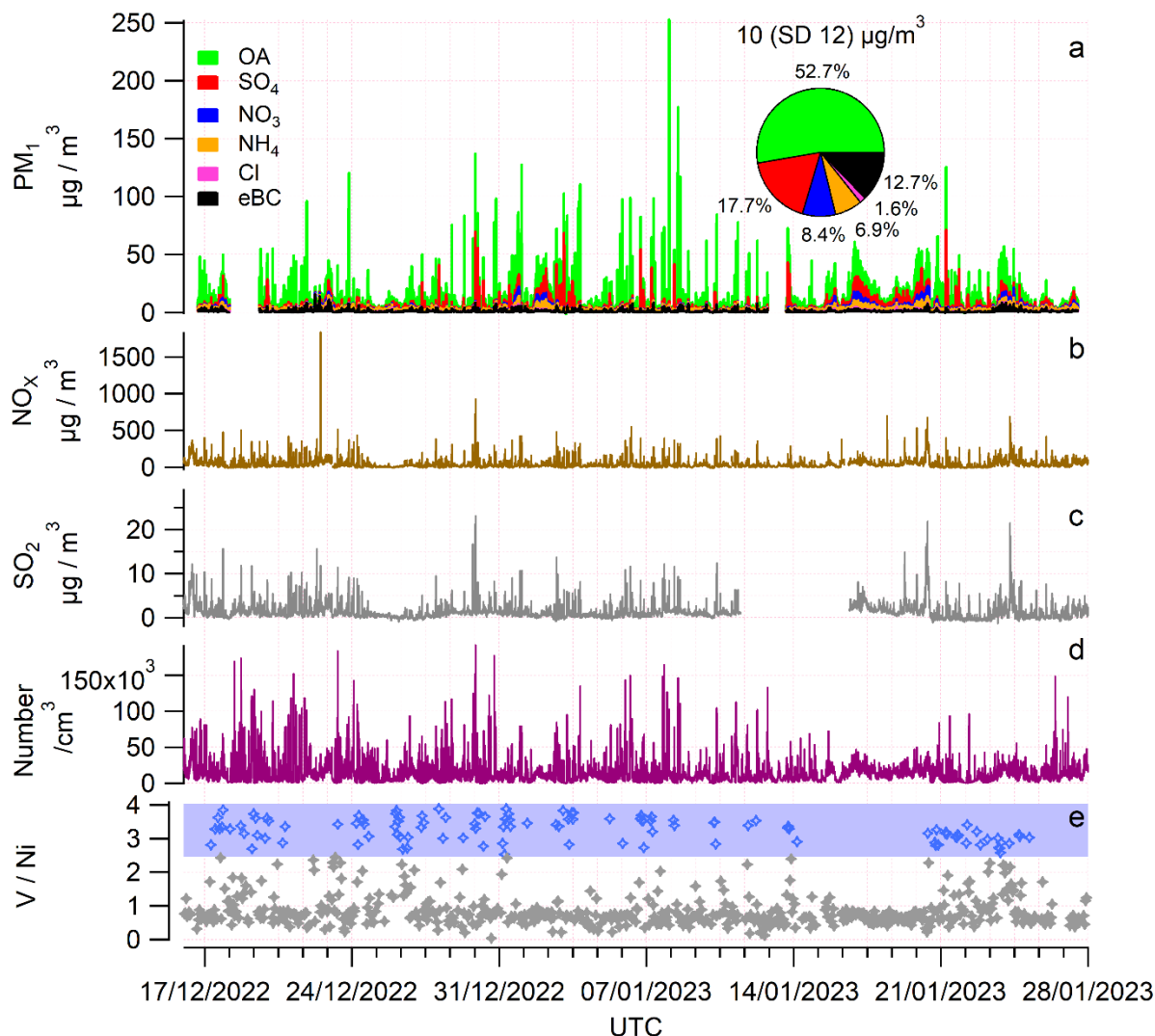
Figure 1: Time series of the high-time resolution ambient measurements during the intensive PortAIR campaign. From top to bottom panels: (a) reconstructed PM$_1$ on the left axis formed from stacked species along with a pie chart of the average contributions of each (above: mean PM$_1$ (standard deviation)); (b) NO$_x$ in brown; (c) SO$_2$ in grey; (d) number concentration of particles from 10-500 nm in dry electrical mobility diameter (d$_m$) from the SMPS; (e) Vanadium to Nickel ratio (V/Ni) as measured by the Xact with blue shaded area denoting the range of V/Ni traditionally associated with HFO and blue markers showing data in the range (grey when not).

3.1 Ship profile identification

To derive a ship emission profile, data time series were used to search for plumes with known markers, namely V/Ni ratios, SO$_2$ and NO$_x$ concurrent spikes, and OA with a mass spectral profile indicative of oil or petrol fuel burning. Since the Xact was measuring at hourly time resolution, the V and Ni data were treated as an indicator of a shipping emission plume within that hour. The presence of concurrent spikes in the higher time resolution SO$_2$ and NO$_x$ data was subsequently used to

255 determine the time and duration of the shipping plumes. Using this approach, around 50 plumes were manually identified with the V/Ni ratio in the expected range for HFO emissions, and occurred when the wind direction was primarily from the South (Southwest to Southeast included), inferring advection of plumes from nearby ferry berths, the marine shipping channel, and South Dublin Port. However, there were many OA-dominated plumes that lacked V and Ni in either significant concentrations or when the ratio was lower than the expected range for HFO. In these cases, the OA-dominated plumes still

260 contained concurrent spikes in SO_2 and NO_x concentrations, occurred when the wind direction came from the South-Western side of the port across a nearby ferry berth, and occurred at times when ships were either in the process of docking or docked. Since the classical V/Ni ratio may no longer be a reliable marker for emissions from ships using low sulfur marine fuels (Anders et al., 2023; Czech et al., 2017), the results obtained here were used to categorise two different types of ship plumes as follows:

265

S-Ship – Sulfate-rich Ship emissions that are characterised by the well documented V/Ni ratio of 2.5–4 associated with HFO, have high elemental sulfur concentrations, and have elevated SO_2 and NO_x concentrations. These pollution spikes are also associated with significant concentrations of particulate SO_4^{2-} relative to OA.

270 **O-Ship** – Organic-rich Ship emissions that are dominated by OA, have elevated SO_2 and NO_x concentrations, but do not have the V/Ni ratio associated with HFO and with significantly lower V (< 0.04 µg m^{-3}) and Ni (< 0.02 µg m^{-3}) concentrations.

To derive the Q-ACSM mass spectral signatures for S-Ship and O-Ship, five exemplary plumes of each type were selected

275 for detailed analysis. The strict criteria for selecting the exemplary plumes were; (i) mean PM$_1$ concentration was greater than 20 µg m^{-3}, (ii) the Q-ACSM sampled the plume for at least two data points (more than five minutes), (iii) the plume occurred when the two closest ferry ports had ships manoeuvring in and out of docks or docked at port, as confirmed by Dublin Port shipping logs, and the wind direction was from these respective locations. Additionally, the selected plumes had significantly high OA and SO_2 concentrations, but were isolated plumes without overlapping regional pollution. The

280 characteristics of the exemplary plumes are described in Table S1. The five exemplary S-Ship plumes had an average PM$_1$ concentration of 61 ± 36 µg m^{-3}, with the following composition; SO_4^{2-} (52%), OA (41%), eBC (6%), NO_3^- (1%), Cl$^-$ (0.4%) and near zero NH_4^+ contribution, indicating the plumes were acidic. The five exemplary O-Ship plumes had an average PM$_1$ concentration of 114 ± 29 µg m^{-3}, with the following composition; OA (92.5%), eBC (6%), SO_4^{2-} (2%), NO_3^- (0.4%), Cl$^-$ (0.2%), and NH_4^+ (0.2%). These O-Ship plumes were also acidic with extremely low NH_4^+ contribution. The OA mean ship

285 profiles are compared in Fig. S7a. While the OA mass spectrum (UMR) was similar (r^2=0.688), S-Ship contained more signal intensity at m/z 15, 17, 18, 27, 44. Yet, it was apparent that the S-Ship and O-Ship mass spectral profiles of OA showed low variance from each other, which could make them hard to distinguish by PMF if only the OA ions are used in the model matrix. Since S-Ship emissions also had a very strong SO_4^{2-} contribution, the combined OA and SO_4^{2-} data was

used to derive the final ship profiles (Fig. 2). O-Ship SO_4^{2-} ions were present at low relative contributions, but since the profile did not show any realistic fragmentation pattern (SO $8.24x \times 10^{-3}$, SO_2 4.96×10^{-3}, SO_3 5.23×10^{-3}, HSO_3 1.505×10^{-2}, and H_2SO_4 -9.96×10^{-4}) the ion fragments were set to zero with standard deviation shown in Fig. 2. A comparison was made between the S-Ship and O-Ship mass spectral profiles obtained in this work with the ship profile derived from ACSM measurements in Dunkerque, France (Zhang, 2016), which is also in a SECA zone. The O-Ship profile compared extremely well ($r^2 = 0.986$) to the Ship-like OA (Sh-OA) profile obtained in Dunkerque (Fig. S13) and confirms O-Ship and (Sh-OA) as a good reference profile for low-S ship fuel emissions.
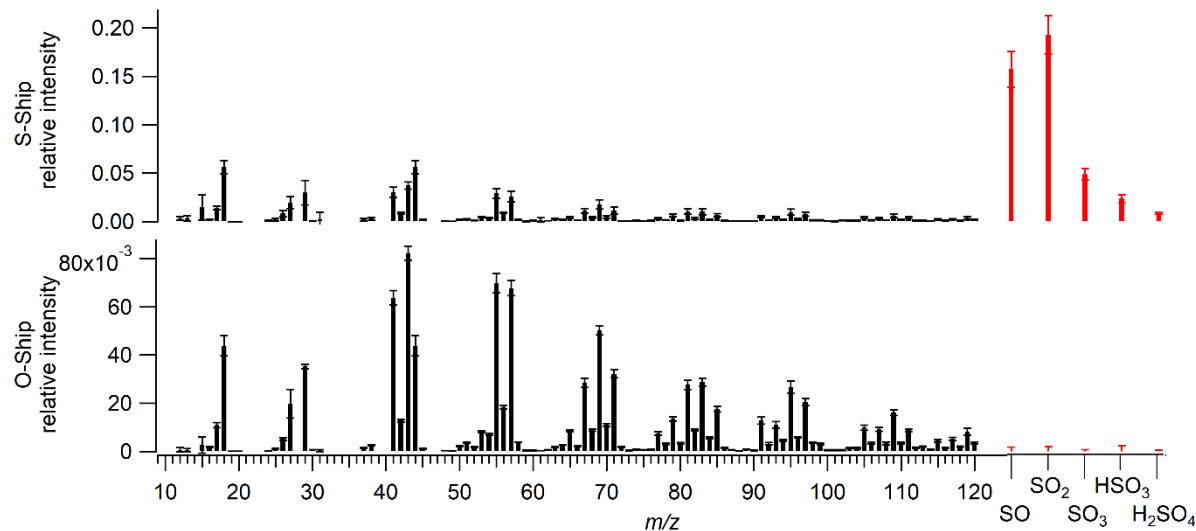
Figure 2: Reference mass spectra profiles of S-Ship (top) and O-Ship (bottom) plumes. The OA mass spectra are shown in black. The sulfate-related ions SO^+, SO_2^+, SO_3^+, HSO_4^+, and $H_2SO_4^+$ (*m/z* 48, 64, 80, 81, and 98, respectively (see methods in Sun et al. (2012)) are shown in red and placed at *m/z* 125, 130, 135, 140, and 145, respectively to run PMF. Error bars indicate the standard deviation of the sample from mean for the five exemplary plumes.

3.2 Organic-sulfate source apportionment

3.2.1 PMF results

Unconstrained PMF solutions with 2–10 factors were tested as a first step (see Supplementary discussion S1.1). Only the two-factor solution resulted in reasonable profiles, comprised of generic hydrocarbon-like organic aerosol (HOA) and an aged organic aerosol. The rest of the solutions resulted in some particular ions separating out as individual factors that, however, are not physically meaningful. Despite the measurements being conducted in a port environment, no sea salt factor (see Supplementary) was resolved by the unconstrained PMF solution for the intensive campaign period. This was supported by evaluation of elemental Cl (Xact) that showed comparable contributions from the directions of the city and of the sea.

To direct the PMF model towards a physically meaningful solution, the mass spectra of reference primary OA factors were constrained using the ME-2 algorithm (Canonaco et al., 2013). The organic-sulfate combined PMF was run by combining the two constrained ship type factors with other constrained factors expected to be present. These include a traffic hydrocarbon-like-organic-aerosol (HOA) derived from a previous curb side study in Dublin, Ireland (see Fig. S8) (Lin et al., 2020), as well as individual solid fuel burning (SFB) factors for peat, wood, and coal from a previous Irish study (Lin et al., 2021), a sea-salt factor, and the S-Ship and O-Ship factors discussed above. While finding the most reasonable solution is somewhat subjective, the best solution occurs when increasing the number of factors leads to avoidable splitting of the factors or when reducing the number of factors leads to avoidable mixing of factors. Whether factors are split or mixed in a solution was evaluated by looking at correlations to other factors as well as external time series (e.g. NO_3^-, NH_3^+, eBC, metals, etc.) and checking if diurnal patterns looked representative of real port or city activities (e.g. traffic patterns). The best solution was determined to be with 6-factors, two unconstrained and four constrained factors: S-Ship emissions, O-Ship emissions, Peat, and traffic HOA. Increasing the number of factors for the ME-2 solution beyond six could not resolve any more reasonable solutions, with extra factors being separated into unrealistic profiles with poor correlation to external tracers. The six-factor solution was then run with bootstrap resampling (50 runs) and found to be very stable, where the standard deviation of the profiles or time series was 2-23%. The factor profiles derived from the 6-factor bootstrap solution for the organic-sulfate source apportionment are shown as factor profiles in Fig. 3a. The time series and diurnal trends for the four constrained factors (S-Ship, O-Ship, HOA, Peat) and the two unconstrained factors (OOA, X-Ship) are presented in Fig. 3b and Fig. 3c, respectively.

The diurnal variations (Fig. 3c) between the S-Ship and O-Ship factors were similar, while the time series shows differences in the patterns observed for the factors, as well as some periods where the factors overlap but peak at slightly different times. This may indicate intrinsically linked emissions from different emission sources. The HOA factor had a diurnal pattern with small peaks occurring at the same times as the peaks in the ship factors, which is not surprising given the flow of vehicular traffic linked with ship arrivals and departures. However, the HOA factor also had an evening peak, which could be caused by the HOA traffic mass spectra being very similar to those for home heating oil at UMR and $m/z < 120$ (Lin et al., 2020). The correlation matrices (Fig. S9) showed HOA correlating with SFB-related factors (peat, OOA) and elemental tracers (As and K), as well as with shipping-related tracers (i.e. SO_2 and the X-Ship factor). The HOA factor seemed split between traffic from the port and a city source that peaks in the evening, likely oil burning for residential heating. Peat showed time trends that match the regional pollution episodes in Fig. S6, and diurnal patterns that are dissimilar to the ship emissions, with a clear evening peak. The increase in the evening is expected for factors associated with residential SFB for home heating.

One of the unconstrained factors is attributed to oxygenated OA (OOA). This factor followed a very similar diurnal pattern
and time series to Peat, which points to OOA being present or produced during SFB pollution episodes. The factor
correlation matrix (Fig. S9) also supports this assertion, with strong correlations for OOA with Peat (r = 0.74), elemental As
(r = 0.64), elemental K (r = 0.62), and Cl$^-$ (r = 0.62) potentially related to the build-up of local pollution, which can be
dominated in winter by SFB related pollution (e.g. Lin et al. (2023)). On the other hand, the correlation of OOA with NO$_3^-$,
NH$_4^+$ and Cl$^-$ could be related to regional pollution during stagnant weather, so all or some portion of OOA may be
independent of SFB. The strong correlation of OOA with NO$_3^-$ (r = 0.77) could indicate the OOA was semi-volatile, freshly
formed secondary OA, which would point to the formation of OOA along the route to the port. As a result, OOA is probably
a combination of contributions from regional secondary production, including from SFB sources, and freshly formed
secondary aerosol.
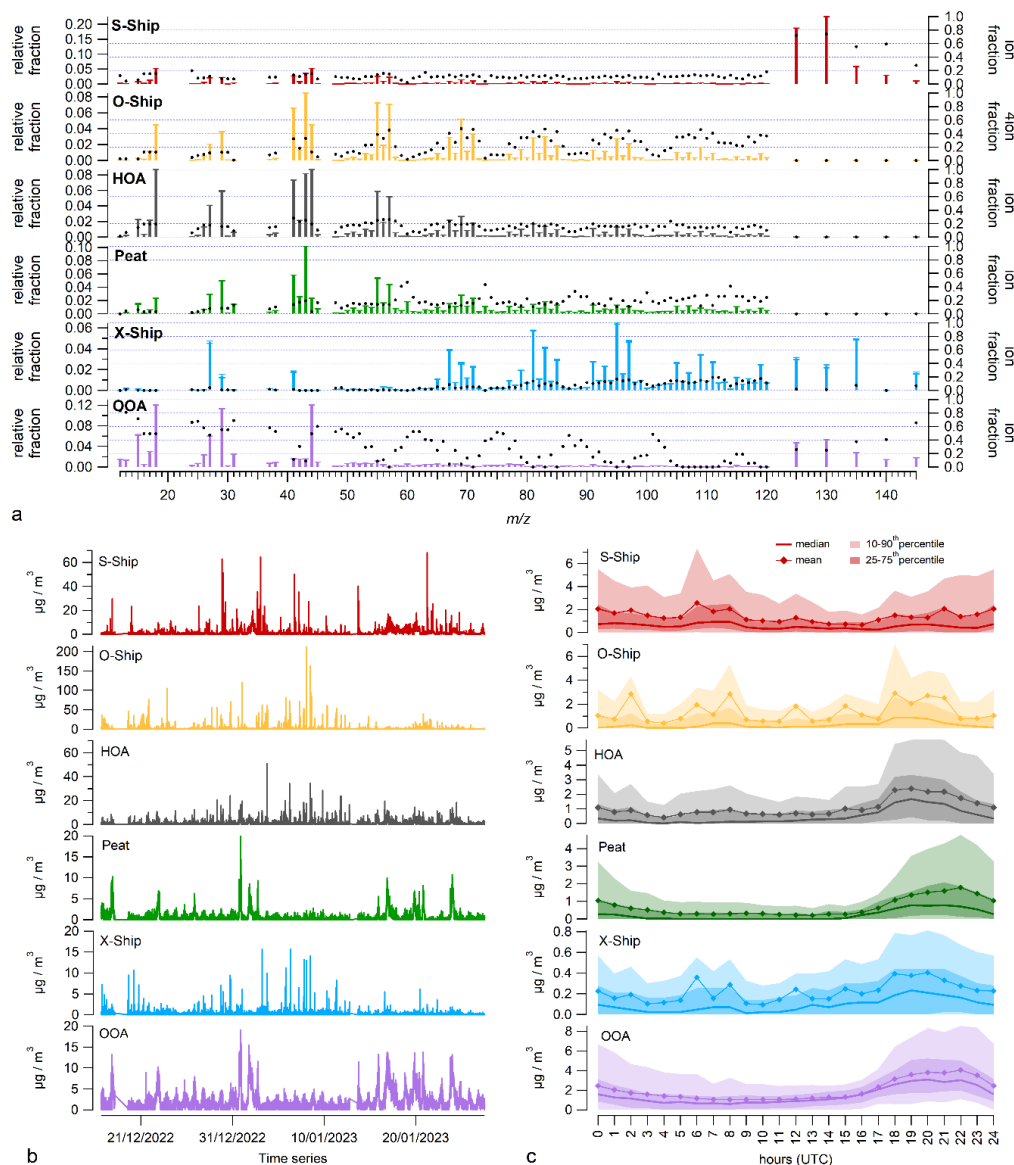
Figure 3: The 6-factor PMF solution showing (a) factor profiles, (b) the factor times series and (c) the diurnal profiles. The colors of each factor are consistent throughout; S-Ship in red, O-Ship in orange, HOA in charcoal, Peat in green, X-Ship in blue, and OOA in purple. In (a), the left axis is the relative ion fraction of the mass spectrum, with error bars indicating the variation from the bootstrap resampling. Right axis is the relative ion fraction of each *m/z* in that profile compared with the total for that *m/z* (markers). In (b), the left axis shows mass concentration (µg m⁻³) as a function of time for each factor. In (c), the left axis shows the median and mean diurnal cycle of the full time series with 25-75th percentiles (dark shaded) and 10-90th percentiles (light shaded) indicated.

The other unconstrained factor contained heavier ions, without fragmentation at lower *m/z* that would be associated with further fragmentation of the molecular clusters, and lacked *m/z* 44, indicating no ageing. This factor time series closely matched peaks in the time series of O-Ship, and to a lesser extent S-Ship as well, and matched the diurnal profiles of the

shipping related factors. It correlated with O-Ship and to a lesser extent with HOA and S-Ship. It is unlikely to be a split factor due to association with both shipping factors, which points to a source related to ship engines, mostly to vessels using low sulfur fuels. For these reasons, we call this factor the X-Ship factor. The ions at m/z 81 and 95 are typical for exo-sulfur aromatics while there are also $C_nH_{2n-1}^+$ ions for m/z 41 and 55, as well as m/z 105 and 119 that could be carboxylic acids,

370 possibly naphthenic acid. Some of these ions point towards this split factor being an indicator of engine oil lubricant (Anders et al., 2023; Czech et al., 2017). The X-Ship OA ions are poorly correlated with the S-Ship (r^2 = 0.007) and O-Ship (r^2 = 0.089) factors (see Fig. S7b and Fig. S7c). In both cases, the majority of X-Ship ions, especially at higher m/z, have stronger relative intensities. The major difference is that X-Ship does not contain m/z 18, 41, 43, 44, 55, and 57, indicating a lack of hydrocarbon content and ageing. The X-Ship factor also appeared in unconstrained PMF runs of the matrices, therefore, it

375 was mathematically divergent and found in most solutions with a few unconstrained factors.

3.2.2 Source apportioned ship plumes

The organic-sulfate PMF resolved 58 S-Ship plumes and 190 O-Ship plumes over the intensive campaign. The average chemical breakdown of PM_1, along with NO_x and SO_2, is shown in Fig. 4b for S-Ship and Fig. 4c for O-Ship. S-Ship factor plumes were comprised mostly of SO_4^{2-} (57%), followed by OA (35%), eBC (6%), NO_3^- (1%), with negligible contributions

380 from NH_4^+ and Cl^-. There is slightly more SO_4^{2-} and less OA than the average of the exemplary S-ship plumes, caused by the inclusion of plumes with lower PM_1 concentrations. O-Ship plumes were comprised mostly of OA (77%), followed by eBC (9%), SO_4^{2-} (7%), NO_3^- (3%), NH_4^+ (3%) and Cl^- (1%). The increased contribution from inorganic species compared to the average of the exemplary O-Ship plumes is caused by the presence of plumes on top of regional secondary aerosol. Overall, 7% of the S-Ship plumes and 27% of O-Ship plumes had PM_1 concentrations less than 15 µg m^{-3}. The 99th percentile of PM_1

385 statistically represents extreme pollution episodes, which was PM_1 > 53.5 µg m^{-3} during the PortAIR intensive campaign. The O-Ship factor included 33 plumes where PM_1 reached at least 53.5 µg m^{-3} (99th percentile of PM_1). Whereas the S-Ship factor only had 10 plumes where PM_1 reached 53.5 µg m^{-3}.

Using the PMF solution to identify S-Ship and O-Ship plumes, particle mass concentration and other components of these

390 two Ship factor types can also be compared. In the PMF solution, despite the higher frequency of occurrences of O-Ship pollution plumes, S-Ship and O-Ship plumes had nominal average PM_1 concentrations of 29 ± 22 µg m^{-3} and 32 ± 26 µg m^{-3}, respectively. This was due to S-Ship pollution events having significant fractions of SO_4^{2-}, such that mean OA was 10 ± 10 µg m^{-3} and mean SO_4^{2-} was 17 ± 12 µg m^{-3} for S-Ship. O-Ship however had 25 ± 24 µg m^{-3} of OA and 2 ± 2 µg m^{-3} of SO_4^{2-} on average. S-Ship PM_1 ranged from 9-135 µg m^{-3} and O-Ship ranged from 4–252 µg m^{-3}.

395

Average particle number concentrations were 1.52 ± 1.55 × 10^4 cm^{-3} and 3.75 ± 2.28 × 10^4 cm^{-3} for S-Ship and O-Ship respectively. Although the number concentration varied widely across the ship plumes, on average O-Ship had more particles associated with the plume type. Additionally, while there were variations in size modal distributions over the

duration of the plume and larger variation from plume to plume, the number-size distributions of O-Ship emissions were
400   shifted to smaller sizes than S-Ship (Fig. S10). The combined smaller diameter particles at higher number concentration
from O-Ship could have more adverse health impacts as these particles (d_m < 100 nm) penetrate into the bloodstream and
translocate to all organs in the body (Schraufnagel, 2020).

In terms of NO_x and SO_2, both median and average values were similar for the two types, with S-Ship plumes having an
405   average concentration of 117.6 ± 118.0 µg m^{-3} of NO_x and 3.5 ± 3.4 µg m^{-3} of SO_2 and O--Ship having an average of 132.3 ±
108.7 µg m^{-3} of NO_x and 3.9 ± 3.2 µg m^{-3} of SO_2. The eBC concentrations were also similar with S-Ship having 1.8 ± 1.4 µg
m^{-3} and O-Ship having 3.0 ± 1.8 µg m^{-3} of eBC on average. The V/Ni median ratio for S-Ship events was 3.41 (range 2.7–
3.9) in line with the literature, but was 0.74 (range 0–2.3) for O-Ship, which is in line with a study that found V/Ni = 0.6–1.1
after the Global Sulfur Cap 2020 regulation (Tauchi et al., 2022). All the ship emission types can be found summarized in
410   Table S2.

3.2.3 Quantification of sources

Factors from the PMF, inorganic species, and eBC were used to quantify the relative contribution of sources (breakdown
shown in Fig. 4a). This quantification is explained below. Where possible, primary combustion emissions were categorised
by fuel type. The S-Ship factor and OOA factor contained all significant fractions of the SO_4^{2-} ions (Fig. 3a), so these factors
415   were affected by the re-addition of the non-measured SO_4^{2-} fragments (see Sect. 2.3 and supplementary discussion). The PM_1
breakdown using these factors is shown in Supplementary Fig. S11.

The PMF solution has trouble separating the regional SO_4^{2-} from S-Ship SO_4^{2-}. This is partly because the measured SO_4^{2-}
ions have low variability in the ACSM mass spectra, with ammonium sulfate and acidic sulfate having similar relative
420   intensities (Chen et al., 2019) and fragmentation patterns (see discussion in supplementary material and Fig. S14). The
overall effect on the data is that the relative fraction of S-Ship is overestimated by about 8% of the total. While the
separation of regional and ship sulfate is a limitation of the organic-sulfate PMF, the contribution of regional sulfate was
subtracted from the S-Ship factor to isolate HFO emissions.
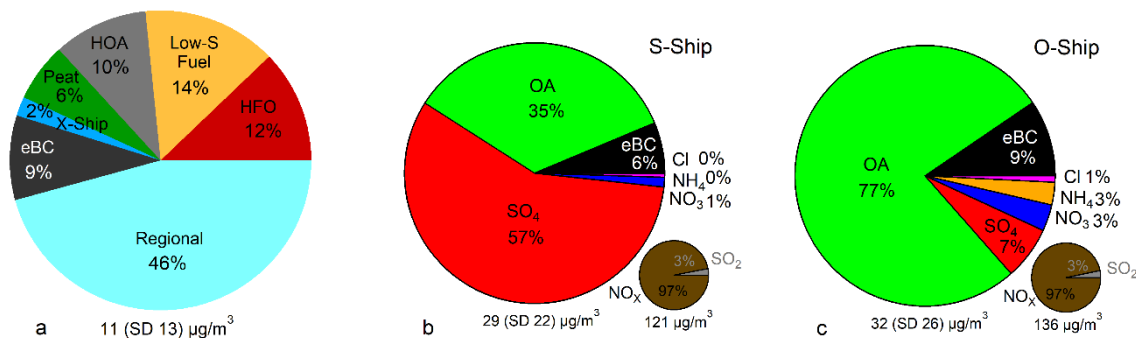
425

Figure 4: Pie charts of the composition breakdown of the (a) source apportioned PM₁ data, (b) S-Ship plumes breakdown of PM₁ measured with gas data pie of SO₂ and NOₓ, and (c) the same for O-Ship.

Since eBC is observed to be part of the ship emissions, it was apportioned to the S-Ship and O-Ship factors using the estimated $eBC/(OA+SO_4^{2-})$ ratios (eBCr). The ratios from the observed five exemplary plumes for S-Ship (eBCr = 0.066) and O-Ship (eBCr = 0.047) were compared to those derived from the source apportioned S-Ship and O-Ship plumes. The S-Ship was comparable with an average eBCr of 0.068, close to 0.066 from the S-Ship five exemplary plumes. However, the O-Ship eBCr differed from 0.047 for the five exemplary plumes to an average of 0.113 for the source apportioned plumes. This difference was caused by the much larger OA contribution during the exemplary plumes than for the average taken over all O-Ship factor plumes. Therefore, one ratio was applied for all O-Ship plumes where $PM_1 > 53.5$ µg m^{-3}, and for the rest of the period another ratio was applied, eBCr = 0.063 and eBCr = 0.141, respectively. These eBCr ratios were used to re-apportion eBC, amounting to 11% of total eBC to HFO (S-Ship) and 13% to low-S fuels (O-Ship). The eBC shown in the pie chart (Fig. 4a) reflects a subtraction of the 24% of eBC (only 2.9% of PM₁) already accounted for in the ship fuels.

Factors and chemical components that belong to regional sources were combined and called Regional source, which includes the OOA, NO_3^-, NH_4^+, Cl$^-$, and regional sulfate subtracted from S-Ship. Just to note, an estimated 1% of PM₁ from the combined NO_3^-, NH_4^+, and Cl$^-$ could be associated with low-S fuel emissions rather than Regional, however, there was enough uncertainty in this estimation that the 1% has been left associated with Regional. The HFO and low-S fuel contains the apportioned eBC, as explained above. Across the campaign, the source contributions to the measured PM₁ were Regional (46%), Low-S Fuel ship emissions (14%), HFO ship emissions (12%) HOA due to traffic or oil burning (10%), non-ship fuel eBC (9%), Peat (6%), and X-Ship emissions (2%). The Dublin Port ship-related factors made up 28% (HFO, low-S Fuel, and X-Ship) of PM₁, not counting ship traffic related HOA and associated traffic eBC. It was difficult to attribute the HOA factor in Dublin Port to either ship-related traffic, city traffic, or oil burning for residential heating. Therefore, we estimate shipping-related emissions in Dublin Port contributed 28–47% of PM₁ (Fig. 4a), as some significant portion of the hydrocarbon-like organic aerosol (HOA) and traffic-related eBC was expected to also come from shipping-related activities such as ferry traffic, vehicles for moving containers, and crane engines.

3.3 Ship emissions when manoeuvring and hoteling

With the unique methodology in this study, PMF was able to identify and separate O-Ship and S-Ship plumes, which are directly related to emissions from vessels operating low-S fuel and HFO respectively. This allowed the frequency of the different ship emissions to be evaluated (low-S frequency > HFO frequency), and also enables the emissions from individual vessels to be investigated, using shipping log information. In Dublin Port, ship manoeuvring takes on average 30 ± 10 minutes from the outer buoy to docking. Additionally, there is no shore power or 'electric ironing' at dock in Dublin Port, so the ships effectively run their engines or generators at dock, called 'hoteling'. The emissions from ships are different during manoeuvring, both because the engine is under a different load compared to hoteling or cruising (Anderson et al., 2015; Liu et al., 2018) and because it is common for ships to switch to different engines and fuels after docking (typically MGO in Dublin Port). Therefore, when meteorological conditions were steady, the manoeuvring in and out of dock showed distinct plumes, with idling periods in between, resulting in time series of both mass and number concentration that resembled the shape of a 'bat ear' (Fig. 5). The bat ear profiles are characterised by intense plumes of PM_1, NO_x and SO_2 during inbound and outbound manoeuvring with a large drop in concentration in between where PM_1 fell typically below 15 µg m^{-3} and the gas concentrations also dropped but remained elevated above background.
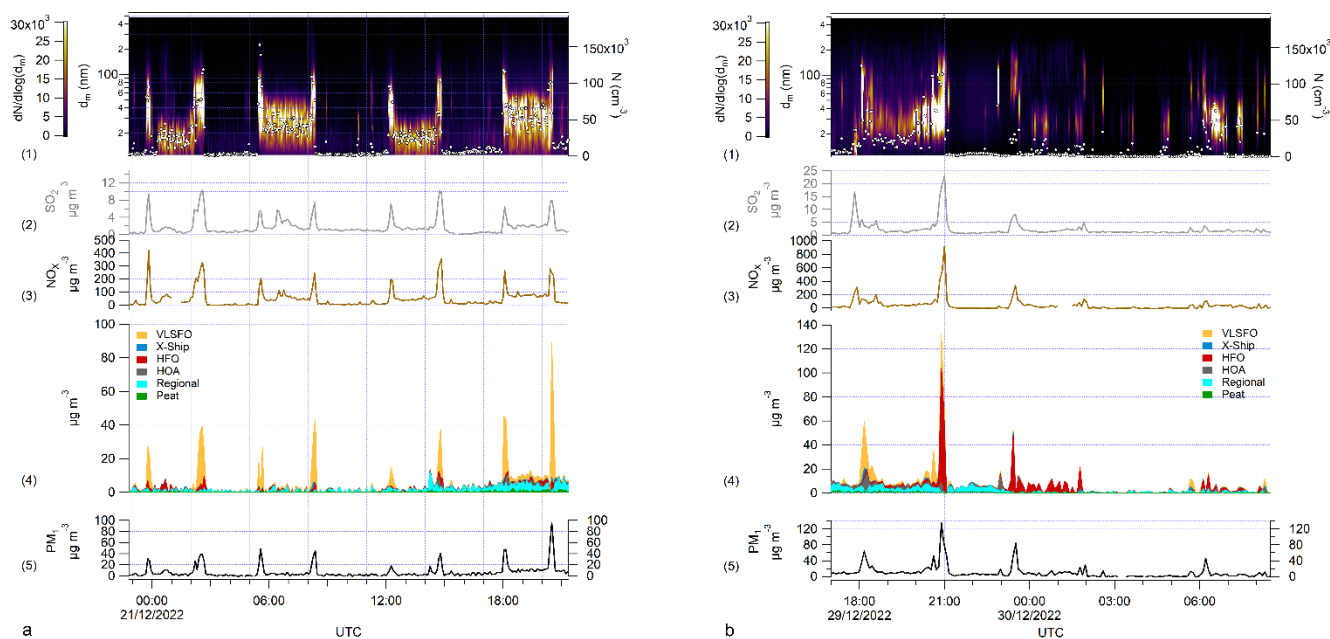
Figure 5: Time series of data during 'bat ear' ship emission events for (a) VLSFO-MGO-VLSFO plumes and (b) some VLSFO and HFO plumes. Panel (1) shows a curtain plot of particle number-size distribution data with particle diameter (d_m (nm)) (left axis) and lognormal concentration ($dN/dlog(d_m)$) indicated by color. The particle number concentration (cm^{-3}) is overlaid with circle markers (right axis). Panel (2) shows shows SO_2 data (grey) and (2) shows NO_x data (brown). Panel (3) shows stacked sources (as in Fig. 4a), and panel (4) shows PM_1..

The low-S bat ears (Fig. 5a) were often the result of a fuel switch from VLSFO at docking to marine gas oil (MGO) while docked. While low in mass concentration, MGO fuels are visible in the number-size distribution as large concentrations of tiny particles ($d_m < 50$ nm) (Fig. S12). The first and third bat ear profile in Figure 5a were from one specific vessel and the

475 second and fourth from another, which may reflect differences in the fuel or engine design. Fewer bat ears attributed to scrubbed HFO emissions were captured due to the lower frequency of these vessels and changing meteorology, but a few are shown in Fig. 5b. At the start of the time series in Figure 5b, the wind direction is transitioning from crossing a VLSFO vessel berth to one with a HFO powered vessel. Then the wind direction stays steady. The emissions observed from 23:00 on December 29th to 02:00 on 30th December (Fig. 5b) originate from a vessel that used HFO with a wet scrubber system

480 (closed loop) all the time. This emission profile was created with different engine loads, as fuel type did not change. The proceeding (December 29th ~21:00) and following (30th December ~06:15) HFO bat ear emission profile was from a vessel that used HFO (with scrubber) during manoeuvring and MGO for generators when in port. Overall, these patterns confirm that the low-S fuels emit higher concentrations of particles that are shifted to smaller sizes, while HFO with scrubber systems often emit relatively less particles (as in Fig. S10).

485 **4 Conclusions**

This work shows that a combination of organic-sulfate PMF is effective in identifying and separating ship emissions based on fuel type when scrubbed heavy fuel oil (HFO) and very low sulfur fuel oil (VLSFO) emissions are present and, thus, can help in quantifying their contributions to PM even when mass concentrations are as low as 4 µg m^{-3}. Over the month-long winter intensive campaign, 58 sulfate-rich (S-Ship) plumes and 190 organic-rich (O-Ship) plumes occurred, of which 43 ship

490 plume events reached over 53.5 µg m^{-3} of PM$_1$ (33 O-Ship and 10 S-Ship). Close investigation of source apportionment factors, information on vessel fuel use, wind direction, and shipping logs indicate that the S-Ship relates to ships that use HFO but have a scrubber system, and O-Ship relates to ships that use low-sulfur (low-S) marine fuels, primarily VLSFO. These two distinct types of ship emission profiles enable organic-sulfate source apportionment with the advantage of distinguishing scrubbed HFO emissions from low-S fuel emissions without the use of V/Ni tracers.

495 Ship plumes were observed to last up to 2.5 hours given steady wind direction and fuel use while a ship was in port. Although, the more extreme pollution peaks (PM$_1$ > 53.5 µg m^{-3}) only lasted 5–35 minutes and were specifically caused when ships were manoeuvring in or out of berth. While cold ironing periods at dock were characterised by lower PM emissions, number concentrations remained extremely high for submicron particles ($d_m < 50$ nm), especially when ships were switched over to Marine Gas Oil (MGO) for power. In fact, MGO emissions were only characterised by these large

500 number-concentrations of small particles, as PM from MGO was not as clearly noticeable (PM$_1$ < 15 µg m^{-3}). Overall, shipping-related emissions in Dublin Port contributed 28–47% of PM$_1$ measured in the port location. There were also several cases of stagnant and cold weather conditions, lasting days at a time, that resulted in the build-up of regional and city pollutants that were found to contribute 46% of PM$_1$. Despite the transient and short-lived nature of shipping emission

plumes in Dublin Port, however, the ship emissions from HFO with scrubber systems and VLSFO combine to contribute a

505 surprisingly significant fraction of PM_1 and submicron particle number concentration in the port area with a potential to increase even further with the planned port activity expansion.

Code Availability

Software for PMF analyses are run using Igor Pro® from WaveMetrics® (https://www.wavemetrics.com/) and SoFi Pro from Datalystica (https://datalystica.com/sofi-pro/) that are available for purchase.

510 **Data availability**

Raw data from the study as well as details on the analyses are available upon request to the contact author(s) Kirsten N. Fossum (kirstennicole.fossum@universityofgalway.ie) and Jurgita Ovadnevaite (jurgita.ovadnevaite@universityofgalway.ie).

Supplement link:

515 **Author contribution:**

JO, COD, and JW designed the research. KNF, NOS, and SJ, carried out the measurements with technical support from SH, AT and DC. AT and DG supplied the Xact and SB supplied the Q-ACSM. KNF and CL performed the analysis. KNF wrote the paper with support from all authors who commented on the paper.

Competing interests:

520 The authors declare that they have no conflict of interest.

Acknowledgements

This work was funded by the Irish Environmental Protection Agency (EPA) under grant number: 2020-CCRP-LS.6, AC3/AEROSOURCE project, supported by EPA-Ireland and the Department of Environment, Climate and Communications.

525 The PM_1 Q-ACSM used in the intensive campaign was provided by Steigvilė Byčenkienė and Vadimas Dudoitis from the SRI Center for Physical Sciences and Technology, Lithuania.

KNF acknowledges and thanks Doug Worsnop for advice on selection of PMF solution, Teresa Spohn for on-site support during the PortAIR campaign, Eamon McElroy, Ken Rooney, and John Dungan and colleagues in Dublin Port Company for access, ongoing support and port-related information, Stenaline, especially Eamon Fortune, for providing insight, access to
530   facilities, and accommodating the sampling site, and also to representatives from the shipping companies that provided details of ship fuel use.

References

Transport Omnibus 2019, An Phríomh-Oifig Staidrimh - Central Statistics Office, www.cso.ie, 2019.

Agrawal, H., Eden, R., Zhang, X., Fine, P. M., Katzenstein, A., Miller, J. W., Ospital, J., Teffera, S., and Cocker, D. R., III:
535   Primary Particulate Matter from Ocean-Going Engines in the Southern California Air Basin, Environmental Science & Technology, 43, 5398-5402, 10.1021/es8035016, 2009.

Anders, L., Schade, J., Rosewig, E. I., Kroeger-Badge, T., Irsig, R., Jeong, S., Bendl, J., Saraji-Bozorgzad, M., Huang, J.-H., Zhang, F.-Y., Wang, C. C., Adam, T., Sklorz, M., Etzien, U., Buchholz, B., Czech, H., Streibel, T., Passig, J., and Zimmermann, R.: Detection of Ship Emissions from Distillate Fuel Operation via Single-Particle Profiling of Polycyclic
540   Aromatic Hydrocarbons, Environmental Science: Atmospheres, 10.1039/D3EA00056G, 2023.

Anderson, M., Salo, K., Hallquist, Å. M., and Fridell, E.: Characterization of particles from a marine engine operating at low loads, Atmospheric Environment, 101, 65-71, https://doi.org/10.1016/j.atmosenv.2014.11.009, 2015.

Bond, T. C., Doherty, S. J., Fahey, D. W., Forster, P. M., Berntsen, T., DeAngelo, B. J., Flanner, M. G., Ghan, S., Kärcher, B., Koch, D., Kinne, S., Kondo, Y., Quinn, P. K., Sarofim, M. C., Schultz, M. G., Schulz, M., Venkataraman, C., Zhang, H.,
545   Zhang, S., Bellouin, N., Guttikunda, S. K., Hopke, P. K., Jacobson, M. Z., Kaiser, J. W., Klimont, Z., Lohmann, U., Schwarz, J. P., Shindell, D., Storelvmo, T., Warren, S. G., and Zender, C. S.: Bounding the role of black carbon in the climate system: A scientific assessment, 118, 5380-5552, https://doi.org/10.1002/jgrd.50171, 2013.

Canonaco, F., Crippa, M., Slowik, J. G., Baltensperger, U., and Prévôt, A. S. H.: SoFi, an IGOR-based interface for the efficient use of the generalized multilinear engine (ME-2) for the source apportionment: ME-2 application to aerosol mass
550   spectrometer data, Atmos. Meas. Tech., 6, 3649-3661, 10.5194/amt-6-3649-2013, 2013.

Canonaco, F., Tobler, A., Chen, G., Sosedova, Y., Slowik, J. G., Bozzetti, C., Daellenbach, K. R., El Haddad, I., Crippa, M., Huang, R. J., Furger, M., Baltensperger, U., and Prévôt, A. S. H.: A new method for long-term source apportionment with time-dependent factor profiles and uncertainty assessment using SoFi Pro: application to 1 year of organic aerosol data, Atmos. Meas. Tech., 14, 923-943, 10.5194/amt-14-923-2021, 2021.

555   Chazeau, B., El Haddad, I., Canonaco, F., Temime-Roussel, B., D'Anna, B., Gille, G., Mesbah, B., Prévôt, A. S. H., Wortham, H., and Marchand, N.: Organic aerosol source apportionment by using rolling positive matrix factorization: Application to a Mediterranean coastal city, Atmospheric Environment: X, 14, 100176, https://doi.org/10.1016/j.aeaoa.2022.100176, 2022.

Chen, G., Canonaco, F., Tobler, A., Aas, W., Alastuey, A., Allan, J., Atabakhsh, S., Aurela, M., Baltensperger, U.,
Bougiatioti, A., De Brito, J. F., Ceburnis, D., Chazeau, B., Chebaicheb, H., Daellenbach, K. R., Ehn, M., El Haddad, I.,
Eleftheriadis, K., Favez, O., Flentje, H., Font, A., Fossum, K., Freney, E., Gini, M., Green, D. C., Heikkinen, L., Herrmann,
H., Kalogridis, A.-C., Keernik, H., Lhotka, R., Lin, C., Lunder, C., Maasikmets, M., Manousakas, M. I., Marchand, N.,
Marin, C., Marmureanu, L., Mihalopoulos, N., Močnik, G., Nęcki, J., O'Dowd, C., Ovadnevaite, J., Peter, T., Petit, J.-E.,
Pikridas, M., Matthew Platt, S., Pokorná, P., Poulain, L., Priestman, M., Riffault, V., Rinaldi, M., Różański, K., Schwarz, J.,
Sciare, J., Simon, L., Skiba, A., Slowik, J. G., Sosedova, Y., Stavroulas, I., Styszko, K., Teinemaa, E., Timonen, H.,
Tremper, A., Vasilescu, J., Via, M., Vodička, P., Wiedensohler, A., Zografou, O., Cruz Minguillón, M., and Prévôt, A. S. H.:
European aerosol phenomenology − 8: Harmonised source apportionment of organic aerosol using 22 Year-long
ACSM/AMS datasets, Environment International, 166, 107325, https://doi.org/10.1016/j.envint.2022.107325, 2022.

Chen, Y., Xu, L., Humphry, T., Hettiyadura, A. P. S., Ovadnevaite, J., Huang, S., Poulain, L., Schroder, J. C., Campuzano-
Jost, P., Jimenez, J. L., Herrmann, H., O'Dowd, C., Stone, E. A., and Ng, N. L.: Response of the Aerodyne Aerosol Mass
Spectrometer to Inorganic Sulfates and Organosulfur Compounds: Applications in Field and Laboratory Measurements,
Environmental Science & Technology, 53, 5176-5186, 10.1021/acs.est.9b00884, 2019.

Collins, D. R., Cocker, D. R., Flagan, R. C., and Seinfeld, J. H.: The Scanning DMA Transfer Function, Aerosol Science and
Technology, 38, 833-850, 10.1080/027868290503082, 2004.

Crippa, M., El Haddad, I., Slowik, J. G., DeCarlo, P. F., Mohr, C., Heringa, M. F., Chirico, R., Marchand, N., Sciare, J.,
Baltensperger, U., and Prévôt, A. S. H.: Identification of marine and continental aerosol sources in Paris using high
resolution aerosol mass spectrometry, Journal of Geophysical Research: Atmospheres, 118, 1950-1963,
doi:10.1002/jgrd.50151, 2013.

COST Action CA16109 COLOSSAL Chemical On-Line cOmposition and Source Apportionment of fine aerosoL, Working
Group 1. Quadrupole Aerosol Chemical Speciation Monitor (Q-ACSM) - Standard Operating Procedure. Deliverable 1.1.
Released in May 2021. https://www.actris-ecac.eu/pmc-non-refractory-organics-and-inorganics.html.

Crippa, M., Canonaco, F., Lanz, V. A., Äijälä, M., Allan, J. D., Carbone, S., Capes, G., Ceburnis, D., Dall'Osto, M., Day, D.
A., DeCarlo, P. F., Ehn, M., Eriksson, A., Freney, E., Hildebrandt Ruiz, L., Hillamo, R., Jimenez, J. L., Junninen, H.,
Kiendler-Scharr, A., Kortelainen, A. M., Kulmala, M., Laaksonen, A., Mensah, A. A., Mohr, C., Nemitz, E., O'Dowd, C.,
Ovadnevaite, J., Pandis, S. N., Petäjä, T., Poulain, L., Saarikoski, S., Sellegri, K., Swietlicki, E., Tiitta, P., Worsnop, D. R.,
Baltensperger, U., and Prévôt, A. S. H.: Organic aerosol components derived from 25 AMS data sets across Europe using a
consistent ME-2 based source apportionment approach, Atmos. Chem. Phys., 14, 6159-6176, 10.5194/acp-14-6159-2014,
2014.

Czech, H., Schnelle-Kreis, J., Streibel, T., and Zimmermann, R.: New directions: Beyond sulphur, vanadium and nickel –
About source apportionment of ship emissions in emission control areas, Atmospheric Environment, 163, 190-191,
https://doi.org/10.1016/j.atmosenv.2017.05.017, 2017.

Davison, A. C. and Hinkley, D. V.: Bootstrap Methods and their Application, Cambridge Series in Statistical and Probabilistic Mathematics, Cambridge University Press, Cambridge, DOI: 10.1017/CBO9780511802843, 1997.

DPC: Dublin Port Masterplan 2040; Reviewed 2018, 2018.

595 Drinovec, L., Močnik, G., Zotter, P., Prévôt, A. S. H., Ruckstuhl, C., Coz, E., Rupakheti, M., Sciare, J., Müller, T., Wiedensohler, A., and Hansen, A. D. A.: The "dual-spot" Aethalometer: an improved measurement of aerosol black carbon with real-time loading compensation, Atmos. Meas. Tech., 8, 1965-1979, 10.5194/amt-8-1965-2015, 2015.

Efron, B.: Bootstrap Methods: Another Look at the Jackknife, The Annals of Statistics, 7, 1-26, 10.1214/aos/1176344552, 1979.

600 Eichler, P., Müller, M., Rohmann, C., Stengel, B., Orasche, J., Zimmermann, R., and Wisthaler, A.: Lubricating Oil as a Major Constituent of Ship Exhaust Particles, Environmental Science and Technology Letters, 4, 54-58, 10.1021/acs.estlett.6b00488, 2017.

Fuchs, N. A.: On the stationary charge distribution on aerosol particles in a bipolar ionic atmosphere, Pure and Applied Geophysics, 185-186, https://doi.org/10.1007/BF01993343, 1963.

605 Furger, M., Minguillón, M. C., Yadav, V., Slowik, J. G., Hüglin, C., Fröhlich, R., Petterson, K., Baltensperger, U., and Prévôt, A. S. H.: Elemental composition of ambient aerosols measured with high temporal resolution using an online XRF spectrometer, Atmos. Meas. Tech., 10, 2061-2076, 10.5194/amt-10-2061-2017, 2017.

Healy, R. M., O'Connor, I. P., Hellebust, S., Allanic, A., Sodeau, J. R., and Wenger, J. C.: Characterisation of single particles from in-port ship emissions, Atmospheric Environment, 43, 6408-6414, https://doi.org/10.1016/j.atmosenv.2009.07.039, 610 2009.

Healy, R. M., Hellebust, S., Kourtchev, I., Allanic, A., O'Connor, I. P., Bell, J. M., Healy, D. A., Sodeau, J. R., and Wenger, J. C.: Source apportionment of $PM_{2.5}$ in Cork Harbour, Ireland using a combination of single particle mass spectrometry and quantitative semi-continuous measurements, Atmos. Chem. Phys., 10, 9593-9613, 10.5194/acp-10-9593-2010, 2010.

615 Hong, W.-J., Dong, W.-J., Zhao, T.-T., Zheng, J.-Z., Lu, Z.-G., and Ye, C.: Ambient PM2.5-bound polycyclic aromatic hydrocarbons in Ningbo Harbor, eastern China: seasonal variation, source apportionment, and cancer risk assessment, Air Quality, Atmosphere & Health, 16, 1809-1821, 10.1007/s11869-023-01373-6, 2023.

Lin, C., Ceburnis, D., Trubetskaya, A., Xu, W., Smith, W., Hellebust, S., Wenger, J., O'Dowd, C., and Ovadnevaite, J.: On the use of reference mass spectra for reducing uncertainty in source apportionment of solid-fuel burning in ambient organic 620 aerosol, Atmos. Meas. Tech., 14, 6905-6916, 10.5194/amt-14-6905-2021, 2021.

Lin, C., Ceburnis, D., Xu, W., Heffernan, E., Hellebust, S., Gallagher, J., Huang, R. J., O'Dowd, C., and Ovadnevaite, J.: The impact of traffic on air quality in Ireland: insights from the simultaneous kerbside and suburban monitoring of submicron aerosols, Atmos. Chem. Phys., 20, 10513-10529, 10.5194/acp-20-10513-2020, 2020.

Lin, C., Huang, R.-J., Ceburnis, D., Buckley, P., Preissler, J., Wenger, J., Rinaldi, M., Facchini, M. C., O'Dowd, C., and
625   Ovadnevaite, J.: Extreme air pollution from residential solid fuel burning, Nature Sustainability, 1, 512-517,
10.1038/s41893-018-0125-x, 2018.

Lin, C., Ceburnis, D., Vaishya, A., Trubetskaya, A., Tan, Y., Wang, T., Smith, W., Johnson, R., Xu, W., Monaghan, R. F.
D., O'Dowd, C., and Ovadnevaite, J.: Air quality—climate forcing double whammy from domestic firelighters, npj Climate
and Atmospheric Science, 6, 101, 10.1038/s41612-023-00427-x, 2023.

630   Lin, C., Ceburnis, D., Huang, R. J., Xu, W., Spohn, T., Martin, D., Buckley, P., Wenger, J., Hellebust, S., Rinaldi, M.,
Facchini, M. C., O'Dowd, C., and Ovadnevaite, J.: Wintertime aerosol dominated by solid-fuel-burning emissions across
Ireland: insight into the spatial and chemical variation in submicron aerosol, Atmos. Chem. Phys., 19, 14091-14106,
10.5194/acp-19-14091-2019, 2019.

Liu, Y., Ge, Y., Tan, J., Fu, M., Shah, A. N., Li, L., Ji, Z., and Ding, Y.: Emission characteristics of offshore fishing ships in
635   the Yellow Bo Sea, China, Journal of environmental sciences (China), 65, 83-91, 10.1016/j.jes.2017.02.020, 2018.

Magee Scientific Inc. (2018) 'Aethalometer® Model AE33 User Manual', (August).

Mazzei, F., D'Alessandro, A., Lucarelli, F., Nava, S., Prati, P., Valli, G., and Vecchi, R.: Characterization of particulate
matter   sources   in   an   urban   environment,   Science   of   The   Total   Environment,   401,   81-89,
https://doi.org/10.1016/j.scitotenv.2008.03.008, 2008.

640   Middlebrook, A. M., Bahreini, R., Jimenez, J. L., and Canagaratna, M. R.: Evaluation of Composition-Dependent Collection
Efficiencies for the Aerodyne Aerosol Mass Spectrometer using Field Data, Aerosol Science and Technology, 46, 258-271,
10.1080/02786826.2011.620041, 2012.

Mueller, D., Uibel, S., Takemura, M., Klingelhoefer, D., and Groneberg, D. A.: Ships, ports and particulate air pollution - an
analysis of recent studies, Journal of Occupational Medicine and Toxicology, 6, 31, 10.1186/1745-6673-6-31, 2011.

645   Ng, N. L., Herndon, S. C., Trimborn, A., Canagaratna, M. R., Croteau, P. L., Onasch, T. B., Sueper, D., Worsnop, D. R.,
Zhang, Q., Sun, Y. L., and Jayne, J. T.: An Aerosol Chemical Speciation Monitor (ACSM) for Routine Monitoring of the
Composition and Mass Concentrations of Ambient Aerosol, Aerosol Science and Technology, 45, 780-794,
10.1080/02786826.2011.560211, 2011.

O'Connor, I. P., Allanic, A., Hellebust, S., Kourtchev, I., Healy, R. M., Healy, D. A., Bell, J. M., Wenger, J. C., and Sodeau,
650   J. R.: Composition and Sources of Particulate Air Pollution in a Port Environment, Cork, Ireland, Environmental Protection
Agency & University College Cork, www.epa.ie, 2013.

Ovadnevaite, J., Lin, C., Rinaldi, M., Ceburnis, D., Buckley, P., Coleman, L., Facchini, M. C., Wenger, J., and O'Dowd, C.:
Air Pollution Sources in Ireland; 2016-CCRP-MS.31, National University of Ireland Galway, Istituto di Scienze
dell'Atmosfera e del Clima and University College Cork www.epa.ie, 60, 2021.

655   Paatero, P.: Least squares formulation of robust non-negative factor analysis, Chemometrics and Intelligent Laboratory
Systems, 37, 23-35, https://doi.org/10.1016/S0169-7439(96)00044-5, 1997.

Paatero, P. and Tapper, U.: Positive matrix factorization: A non-negative factor model with optimal utilization of error estimates of data values, Environmetrics, 5, 111-126, 10.1002/env.3170050203, 1994.

Paatero, P., Eberly, S., Brown, S. G., and Norris, G. A.: Methods for estimating uncertainty in factor analytic solutions,
660 Atmos. Meas. Tech., 7, 781-797, 10.5194/amt-7-781-2014, 2014.

Pandolfi, M., Gonzalez-Castanedo, Y., Alastuey, A., de la Rosa, J. D., Mantilla, E., de la Campa, A. S., Querol, X., Pey, J., Amato, F., and Moreno, T.: Source apportionment of PM10 and PM2.5 at multiple sites in the strait of Gibraltar by PMF: impact of shipping emissions, Environmental Science and Pollution Research, 18, 260-269, 10.1007/s11356-010-0373-4, 2011.

665 Parworth, C., Fast, J. D., Mei, F., Shippert, T., Sivaraman, C., Tilp, A., Watson, T. B., and Zhang, Q. J. A. E.: Long-term measurements of submicrometer aerosol chemistry at the Southern Great Plains (SGP) using an Aerosol Chemical Speciation Monitor (ACSM), Atmospheric Environment, 106, 43-55, 2015.

Petzold, A., Ogren, J. A., Fiebig, M., Laj, P., Li, S. M., Baltensperger, U., Holzer-Popp, T., Kinne, S., Pappalardo, G., Sugimoto, N., Wehrli, C., Wiedensohler, A., and Zhang, X. Y.: Recommendations for reporting "black carbon"
670 measurements, Atmos. Chem. Phys., 13, 8365-8379, 10.5194/acp-13-8365-2013, 2013.

Pieber, S. M., El Haddad, I., Slowik, J. G., Canagaratna, M. R., Jayne, J. T., Platt, S. M., Bozzetti, C., Daellenbach, K. R., Fröhlich, R., Vlachou, A., Klein, F., Dommen, J., Miljevic, B., Jiménez, J. L., Worsnop, D. R., Baltensperger, U., and Prévôt, A. S. H.: Inorganic Salt Interference on CO2+ in Aerodyne AMS and ACSM Organic Aerosol Composition Studies, Environmental Science & Technology, 50, 10494-10503, 10.1021/acs.est.6b01035, 2016.

675 Schraufnagel, D. E.: The health effects of ultrafine particles, Experimental & Molecular Medicine, 52, 311-317, 10.1038/s12276-020-0403-3, 2020.

Sun, Y. L., Zhang, Q., Schwab, J. J., Yang, T., Ng, N. L., and Demerjian, K. L.: Factor analysis of combined organic and inorganic aerosol mass spectra from high resolution aerosol mass spectrometer measurements, Atmos. Chem. Phys., 12, 8537-8551, 10.5194/acp-12-8537-2012, 2012.

680 Tauchi, M., Yamaji, K., Nakatsubo, R., Oshita, Y., Kawamoto, K., Itano, Y., Hayashi, M., Hiraki, T., Takaishi, Y., and Futamura, A.: Evaluation of the effect of Global Sulfur Cap 2020 on a Japanese inland sea area, Case Studies on Transport Policy, 10, 785-794, https://doi.org/10.1016/j.cstp.2022.02.006, 2022.

Tong, M., Zhang, Y., Zhang, H., Chen, D., Pei, C., Guo, H., Song, W., Yang, X., and Wang, X.: Contribution of Ship Emission to Volatile Organic Compounds Based on One-Year Monitoring at a Coastal Site in the Pearl River Delta Region,
685 Journal of Geophysical Research: Atmospheres, 129, e2023JD039999, https://doi.org/10.1029/2023JD039999, 2024.

Tremper, A. H., Font, A., Priestman, M., Hamad, S. H., Chung, T. C., Pribadi, A., Brown, R. J. C., Goddard, S. L., Grassineau, N., Petterson, K., Kelly, F. J., and Green, D. C.: Field and laboratory evaluation of a high time resolution x-ray fluorescence instrument for determining the elemental composition of ambient aerosols, Atmos. Meas. Tech., 11, 3541-3557, 10.5194/amt-11-3541-2018, 2018.

690   Ulbrich, I. M., Canagaratna, M. R., Zhang, Q., Worsnop, D. R., and Jimenez, J. L.: Interpretation of organic components from Positive Matrix Factorization of aerosol mass spectrometric data, Atmos. Chem. Phys., 9, 2891-2918, 10.5194/acp-9-2891-2009, 2009.

Viana, M., Amato, F., Alastuey, A., Querol, X., Moreno, T., García Dos Santos, S., Herce, M. D., and Fernández-Patier, R.: Chemical Tracers of Particulate Emissions from Commercial Shipping, Environmental Science & Technology, 43, 7472-695   7477, 10.1021/es901558t, 2009.

Yang, J., Tang, T., Jiang, Y., Karavalakis, G., Durbin, T. D., Wayne Miller, J., Cocker, D. R., and Johnson, K. C.: Controlling emissions from an ocean-going container vessel with a wet scrubber system, Fuel, 304, 121323, https://doi.org/10.1016/j.fuel.2021.121323, 2021.

Yau, P. S., Lee, S. C., Cheng, Y., Huang, Y., Lai, S. C., and Xu, X. H.: Contribution of ship emissions to the fine particulate 700   in the community near an international port in Hong Kong, Atmospheric Research, 124, 61-72, https://doi.org/10.1016/j.atmosres.2012.12.009, 2013.

Zetterdahl, M., Moldanová, J., Pei, X., Pathak, R. K., and Demirdjian, B.: Impact of the 0.1% fuel sulfur content limit in SECA on particle and gaseous emissions from marine vessels, Atmospheric Environment, 145, 338-345, https://doi.org/10.1016/j.atmosenv.2016.09.022, 2016.

705   Zhang, S.: Dynamic analysis, in near field and with a finer temporal resolution, of a sub-micron aerosol in urban situation under industrial influence - Analyse dynamique, en champ proche et à résolution temporelle fine, de l'aérosol submicronique en situation urbaine sous influence industrielle, Université du Littoral Côte d'Opale, 2016.

Zhao, M., Zhang, Y., Ma, W., Fu, Q., Yang, X., Li, C., Zhou, B., Yu, Q., and Chen, L.: Characteristics and ship traffic source identification of air pollutants in China's largest port, Atmospheric Environment, 64, 277-286, 710   https://doi.org/10.1016/j.atmosenv.2012.10.007, 2013.